https://doi.org/10.7494/miag.2023.3.555.71

TOMASZ GÓRAL
STANISŁAW KRAWCZYK
JAN PAWLIK

Possibilities of manufacturing spatial elements using the 135 hardfacing method

3D printing with thermoplastic materials is slowly becoming commonplace as additive manufacturing has gained a large number of dedicated users over the past few years, and the prices of the requisite equipment have significantly dropped. However, in terms of materials, only plastics have enjoyed this popularity. Although metals are, in a sense, thermoplastic materials, their spatial application would require very advanced setups, which in turn generates high costs and complicates process control. This article discusses the possibilities of the additive manufacturing of metal elements using a three-axis numerically controlled plotter combined with a semi-automatic welding machine using the 135 method. The authors also examined the impact of sudden changes in velocity vectors on geometric deviations.

Key words: *135 method, 3D printing, WAAM, hardfacing, additive manufacturing*

1. INTRODUCTION

Additive manufacturing is currently one of the fastest-growing methods for producing complex-shaped parts in single-piece production or when producing prototype parts using so-called rapid prototyping. Additive manufacturing methods involve building parts by applying successive layers that adhere to each other by melting the substrate. In FDM (Fused Deposition Modelling) technology, parts are produced from various thermoplastic materials, such as ABS or biodegradable PLA [1]. This solution is characterized by low prototype production costs, where high strength properties are not required due to the strong anisotropy of the print [2]. In the DMLS (Direct Metal Laser Sintering) process, selective melting of metal powder takes place. This is currently one of the most expensive methods of producing elements [3], with their strength and wear resistance reaching levels comparable to those of forged or cast components [4]. Both 3D printing and DMLS technologies are already being used in industrial applications. As part of the activities of the "Mechanics" Scientific Circle at the AGH University of Science and Technology in Kraków, a plotter-hardfacing machine was designed and built, which allowed the hardfacing of lettering, as shown in Figure 1.

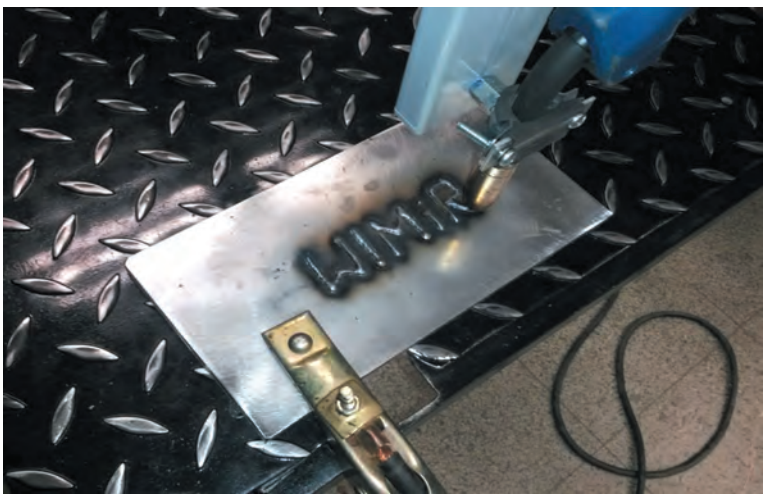

Fig. 1. Hardfaced letters of "WIMiR", which stand for the Faculty of Mechanical Engineering and Robotics at AGH

This device operates similarly to 3D printers using thermoplastic materials in the form of filament, with the difference being that the material in the form of steel welding wire is heated above its melting point not with heaters, but with an electric arc.

2. MATERIALS AND METHODS

For some time now, the hardfacing process using the 135 method has been increasingly popular in additive manufacturing [5, 6]. However, this area still offers room for further research. The main challenges of this method are the difficulties associated with controlling the welding arc and the welding pool, which leads to low geometric and dimensional accuracy of the final product. Another challenge is the three-axis control system. The simplest systems process only one block of CNC code at a time, corresponding to a single coordinate, without analysing the data for the vector to be executed next. After each vector, the process is paused, and the next block is loaded. Due to inertia, the machine reaches the set feed rate only after some time. As a result of using such a control system for a CNC hardfacing machine, the weld bead may have an uneven width, with local thickening, and when hardfacing on a thin substrate, it may even lead to burn-throughs [7]. The problem of speed reduction in CNC devices has largely been eliminated with the introduction of a system for analysing subsequent vectors. This method is called Dynamic Vector Analysis, which increases speed during phases of movement with changing directions (nodes and the start and end of the vector) [8]. This is particularly important for spatial hardfacing of elements with complex shapes. Changing the direction of hardfacing at a constant electrode wire feed rate in these areas causes thickening or even the overflow of liquid metal from the open weld pool.

In this article, the authors conducted research using a modernized 3D hardfacing station, as shown in Figure 2. The station consists of a plotter with an extended arm for mounting the welding torch, NEMA 23 stepper motor drivers, a two-axis screw drive, a MIG 200 MMA semi-automatic welder, and a Fujitsu-Siemens AMILO Pro V2010 computer. The control of the motors and the welding torch was carried out using L289N drivers and Mach 3 Mill software, as shown in Figure 3. Additionally, the welding table was equipped with a resistive preheating system.

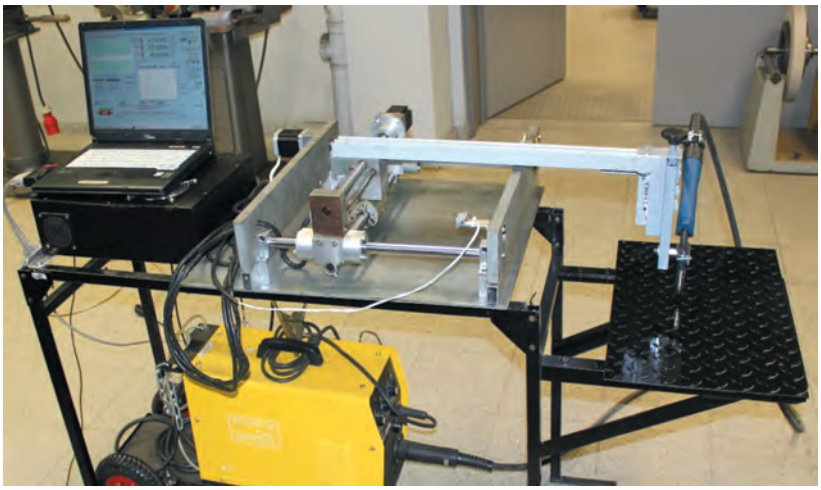

Fig. 2. The spatial hardfacing apparatus built by the "Mechanics" Science Club at the Department of Manufacturing Systems, AGH University of Science and Technology in Krakow

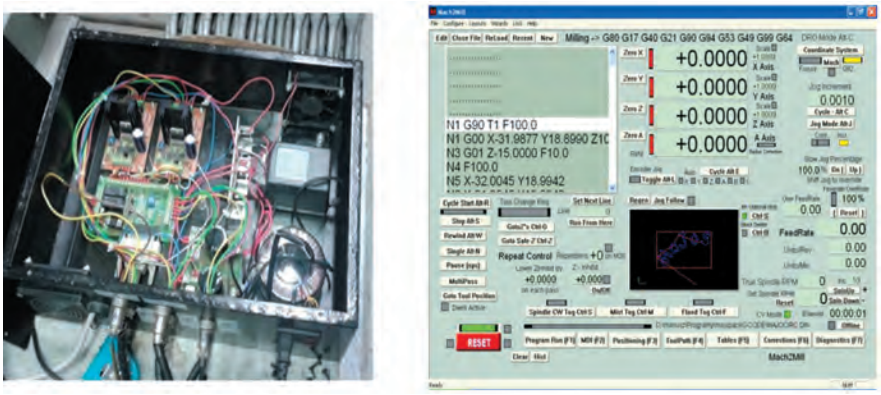

Fig. 3. View of the control box and the Mach2Mill control software

In order to realize a spatial hardfacing process, it was necessary to adjust the current and voltage parameters, as well as the welding and wire feed speed, so that each layer had proper penetration while maintaining the welding pool within the weld seam. Failure to meet this condition resulted in the molten metal flowing off the built structure. Preliminary tests, conducted at a constant welding speed of $V = 7$ m/min and variable electrode feed speed, allowed for the selection of parameters such that the resulting weld beads were uniform in shape and continuous, as shown in Figures 4, 5, and 6. Tables 1, 2, and 3 present the set parameters (where the independent variables were the current intensity I_n and wire feed speed V_{el}) and the measured values, which include voltage, actual current I_s, and the geometric dimensions of the resulting welds in terms of height h and width b of the weld seam.

Table 1

The parameters of the weld beads at a set current of I_n = 100 A. The results are shown in Figure 4

Bead number	Parameters set		Parameters measured		I_s [A]	Geometrical dimensions	
	I_n [A]	V_{el} [m/min]	U_s [mV]	U_s [V]'		*b*	*H*
1	100	4.0	3.31	19.38	33.1	*x*	*X*
2	100	6.5	4.85	19.88	48.5	3.91	1.57
3	100	9.0	6.45	19.78	64.5	4.13	2.07
4	100	11.5	8.02	19.91	80.2	4.63	2.49
5	100	14.0	9.42	19.15	94.2	4.76	2.72

Table 2

The parameters of the weld beads at a set current of I_n = 150 A. The results are shown in Figure 5

Bead number	Parameters set		Parameters measured		I_s [A]	Geometrical dimensions	
	I_n [A]	V_{el} [m/min]	U_s [mV]	U_s [V]'		*b*	*H*
1	150	4.0	4.20	23.57	42.0	*x*	*X*
2	150	6.5	5.44	23.38	54.4	4.69	1.26
3	150	9.0	7.23	23.45	72.3	5.26	1.53
4	150	11.5	8.73	23.86	87.3	5.87	1.77
5	150	14.0	9.74	23.41	97.4	6.27	2.33

Fig. 4. Hardfacing trials at a current of 100 A. The best weld surface was achieved at a wire feed speed of 11.5 m/min

Fig. 5. Hardfacing trials at a current of 150 A

Table 3

The parameters of the weld beads at a set current of $I_n = 200$ A. The results are shown in Figure 6

Bead number	Parameters set		Parameters measured		I_s [A]	Geometrical dimensions	
	I_n [A]	V_{el} [m/min]	U_s [mV]	U_s [V]'		*b*	*h*
1	200	4.0	4.45	26.22	44.5	*x*	*X*
2	200	6.5	6.22	26.53	62.2	4.95	1.22
3	200	9.0	7.22	26.23	72.2	5.84	1.54
4	200	11.5	8.56	26.10	85.6	6.67	1.80
5	200	14.0	9.96	26.07	99.2	7.03	2.23

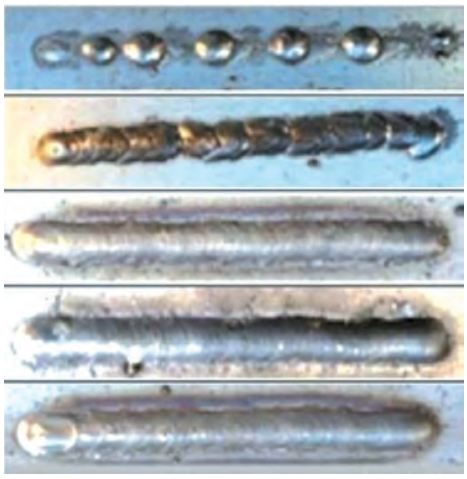

Fig. 6. Hardfacing trials at a current of 200 A

3. 3D SPATIAL HARDFACING

After completing the flat weld beads, the hardfacing machine described in section 2 was used to create three-dimensional objects. During the trial, which involved hardfacing the word WIMIR (shown in Fig. 7), the accumulation of additional material at points where the vector direction of the welding torch speed changed was observed, as mentioned in the introduction. The hardfacing was performed according to the following procedure:

1. Electrical devices were connected to the power source, and their functionality was verified.
2. The table heater was turned on, and a sheet of metal with dimensions 300 × 50 mm and a thickness of 5 mm was placed on it.
3. After the sheet reached a temperature of 120°C, the next steps were taken.
4. The gas cylinders were connected to the welder, the shutoff valve for the gas supply was opened, and the desired flow rate of the shielding gas was set.
5. The computer was started.
6. On the welder's control panel, the preselected parameters were set: current intensity and electrode wire feed speed.
7. The Mach 2 program was launched.
8. The CNC hardfacing machine drivers were activated.
9. The position of the CNC plotter head was zeroed.
10. The appropriate G-code was loaded into the program's memory.
11. The hardfacing process of the element was started.
12. After completing the trials, all devices were turned off, and for safety reasons, the gas cylinders were closed.

Fig. 7. A close-up image of the letters "WIMiR", hardfaced after establishing the right set of parameters

According to the provided procedure, the following were performed:

A. Cylinder with a base diameter of 40 mm
- a shielding gas mixture of 80% argon and 20% CO_2 – M21 mixture was used,
- shielding gas flow rate: 10 l/min,
- SG2 wire with a diameter of 0.6 mm,
- distance from the welding torch to the hardfaced surface: 18 mm,
- welding speed: 360 mm/min,
- current intensity: 100 A,
- wire feed speed: 9 m/min.

B. Prism with a square base with a side length of 40 mm
- a shielding gas mixture of 80% argon and 20% CO_2 was used,
- shielding gas flow rate: 10 l/min,
- SG2 wire with a diameter of 0.6 mm,
- distance from the welding torch to the hardfaced surface: 18 mm,
- welding speed: 420 mm/min,
- current intensity: 100 A,
- wire feed speed: 9 m/min.

C. Prism with an equilateral triangle base with a side length of 40 mm
- a shielding gas mixture of 80% argon and 20% CO_2 was used,
- shielding gas flow rate: 10 l/min,
- SG2 wire with a diameter of 0.6 mm,
- distance from the welding torch to the hardfaced surface: 18 mm,
- welding speed: 500 mm/min,
- current intensity: 100 A,
- wire feed speed: 9 m/min.

Figure 8 shows the multi-layered hardfaced three-dimensional shapes. The inter-bead temperature was not measured.

Fig. 8. The first trials of spatial hardfacing using the MIG/MAG method with the hardfacing machine

4. STUDY OF THE GEOMETRY OF STEEL 3D PRINTS

In order to verify the accuracy of the weld beads, the authors conducted metrological measurements of the geometric dimensions of the weld bead. The previously provided dimensional values pertained to the centre of the path, so to obtain the external dimension, half the width of weld bead number 4 from Table 1 should be added ($b = 4.63$, $1/2 \cdot b = 2.31$).

The expected values of the external dimensions for each of the 3D prints were thus established at 42.3 mm. The authors measured samples at 20 random points, excluding areas with incorrectly made weld beads (shown in the lower part of Figure 9). Subsequently, the standard deviations from the expected value (σ) were calculated. The results of the measurements and calculations are presented below in Table 4.

Geometric errors were most pronounced in the case of the rectangular prism with a square base. The authors conclude that this is due to the presence of 8 segments at the corners where material accumulation occurred. In the case of the cylinder and the prism with a triangular base, lower standard deviations from the nominal dimensions were observed. However, for the cylinder, where the working end had set constant values for the direction change vector, the deviations were noticeably the lowest.

Table 4

Data from the metrological verification of the spatially hardfaced solids

Measurement number	Cylinder with a diameter of 42.3 mm	Prism with a square base and a side length of 42.3 mm	Prism with a triangular base and a side length of 42.3 mm
1.	44.31	43.59	42.80
2.	43.94	44.31	43.30
3.	44.39	44.35	44.68
4.	43.66	44.87	44.62
5.	42.88	45.21	43.76
6.	43.93	45.27	43.78
7.	43.91	44.51	43.07
8.	42.71	44.48	44.19
9.	44.06	44.45	44.45
10.	43.79	43.57	44.26
11.	45.91	45.18	43.50
12.	42.84	45.52	45.66
13.	43.76	45.82	43.71
14.	44.37	45.19	44.09
15.	43.23	45.68	42.02
16.	42.90	45.37	43.30
17.	42.66	46.48	45.48
18.	44.06	45.75	45.44
19.	43.02	44.93	43.94
20.	43.86	44.63	44.57
Mean:	43.7095	44.958	44.031
σ:	1.59942	2.753614	1.950162

Fig. 9. Depicts correctly manufactured spatial hardfaced models (a); illustrates defects resulting from excessively high interlayer temperatures (b). The fragments with defects were not considered in the metrological verification

The authors decided to additionally apply a simple statistical test using Student's *t*-test to check how close the resulting geometry was to the nominal dimensions. The significance level used was $\alpha = 0.05$, and the number of degrees of freedom was $k = n - 1$, which means $k = 19$. By reading the value from the Student's *t*-distribution table, we obtain $t_{0.05;19} = 2.093$. The general formula used is presented below:

$$P\left(\overline{x} - \frac{\sigma \cdot t}{\sqrt{n}} < \overline{m} < \overline{x} + \frac{\sigma \cdot t}{\sqrt{n}}\right) = 0.95 \tag{1}$$

For the cylinder, the calculations are as follows:

$$\begin{aligned} &P\left(43.7095 - \frac{1.59942 \cdot 2.093}{\sqrt{20}} < m_w < 43.7095 + \frac{1.59942 \cdot 2.093}{\sqrt{20}}\right) = 0.95 \\ &P\left(43.7095 - 0.7485 < m_w < 43.7095 + 0.7485\right) = 0.95 \\ &P\left(42.961 < m_w < 44.458\right) = 0.95 \end{aligned} \tag{2}$$

This means that we can assume with 95% probability that the diameter of the actual, spatially hardfaced cylinder will fall within the interval:

$$m_w \in \langle 42.961,\ 44.458 \rangle \tag{3}$$

Similarly, the calculations for the prism with a square base are as follows:

$$\begin{aligned} &P\left(44.958 - \frac{2.753614 \cdot 2.093}{\sqrt{20}} < m_k < 44.958 + \frac{2.753614 \cdot 2.093}{\sqrt{20}}\right) = 0.95 \\ &P\left(44.958 - 1.2887 < m_k < 44.958 + 1.2887\right) = 0.95 \\ &P\left(43.6693 < m_k < 46.2467\right) = 0.95 \\ &m_k \in \langle 43.6693,\ 46.2467 \rangle \end{aligned} \tag{4}$$

The calculations for the prism with a triangular base were conducted similarly as follows:

$$\begin{aligned} &P\left(44.031 - \frac{1.950162 \cdot 2.093}{\sqrt{20}} < m_t < 44.031 + \frac{1.950162 \cdot 2.093}{\sqrt{20}}\right) = 0.95 \\ &P\left(44.031 - 0.9126 < m_t < 44.031 + 0.9126\right) = 0.95 \\ &P\left(43.1184 < m_t < 44.9436\right) = 0.95 \\ &m_t \in \langle 43.1184,\ 44.9436 \rangle \end{aligned} \tag{5}$$

The results are summarized in Table 5, where the symbol "W" denotes the number of sudden changes in direction, *Z* represents the set value, *X* signifies the average value, *R* indicates the difference between the averaged measured value and the set value, *M* represents the range of the measured value with a 95% probability, and *D* denotes the deviation between the mean and the extreme values of the range *M*.

Table 5

Data regarding the geometrical deviations

Shape type	*W* [–]	*Z* [mm]	*X* [mm]	*R* [mm]	*M* [mm]	*D* [mm]
Cylinder	0	42.300	43.710	1.4095	42.961–44.458	0.7485
Prism with square base	3	42.300	44.031	1.7310	43.669–46.270	0.9126
Prism with triangular base	4	42.300	44.958	2.6580	43.118–44.944	1.2887

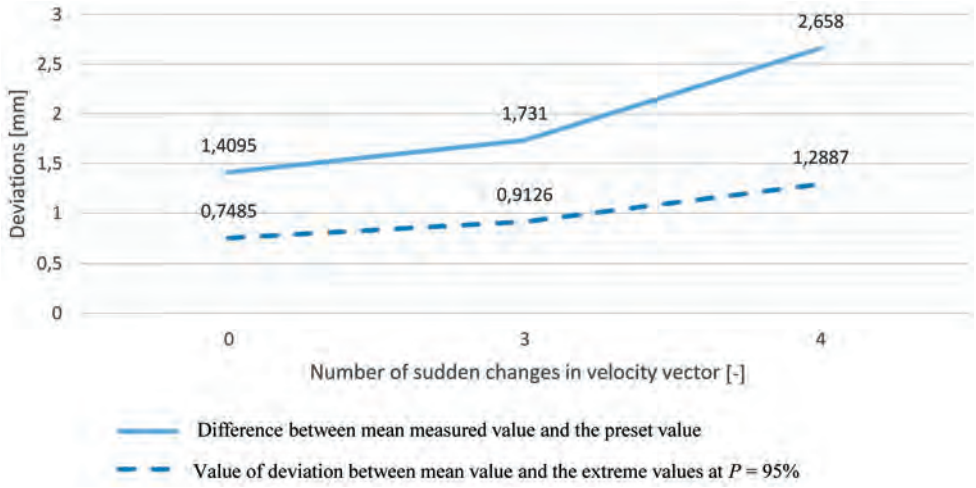

Fig. 10. Graph of geometric deviations as a function of the number of sudden changesin the direction of the velocity vector

The results of the analysis are presented in Figure 10, which shows that as the number of sudden changes in the direction of the welding torch's velocity vector increases, the dimensional discrepancies also increase. Consequently, to substantiate the findings, a one-way ANOVA (Analysis of Variance) was additionally applied. Let the null hypothesis H_0 be stated as:

"The number of sudden changes in the direction of the velocity vector of the welding torch in the current setup has no effect on dimensional inaccuracy with 99% confidence".

The alternative hypothesis H_a will then state:

"The number of sudden changes in the direction of the velocity vector of the welding torch in the current setup has an effect on dimensional inaccuracy with 99% confidence".

Number of degrees of freedom between groups:

$$df_b = k - 1 = 3 - 1 = 2 \tag{6}$$

Number of degrees of freedom within groups:

$$df_b = n_t - k = 60 - 3 = 57 \tag{7}$$

where:

k – sum of groups,

n – sum of measurements taken.

For the determined degrees of freedom of the system, the critical F value was selected from the Fisher distribution table. Its value is $F_{2:57} = 4.998$.

Using the data from Table 4, the mean for all measurements was calculated:

$$\bar{x}_C = \frac{\bar{x}_w + \bar{x}_t + \bar{x}_k}{n}$$
$$\bar{x}_C = \frac{43.7095 + 43.5310 + 44.9580}{3} = 44.06617 \tag{8}$$

The sum of squared deviations from the overall mean $\bar{x}_C$ for all measurement values was also calculated, as well as the sum of squared deviations from the means for individual shapes $\bar{x}_w + \bar{x}_t$ or $\bar{x}_k$. The results of the calculations are presented in Table 6. SS_T denotes the total sum of squares, SS_W denotes the sum of squares within a given group, and SS_B denotes the sum of squares between groups.

$$SS_T = SS_W + SS_B$$
$$SS_T = \sum_{i=0}^{n=20} (x_{wi} - \bar{x}_C)^2 + (x_{ti} - \bar{x}_C)^2 + (x_{ki} - \bar{x}_C)^2 = 67.11$$
$$SS_W = \sum_{i=0}^{n=20} (x_{wi} - \bar{x}_C)^2 + (x_{ti} - \bar{x}_C)^2 + (x_{ki} - \bar{x}_C)^2 = 42.93$$
$$SS_B = SS_T - SS_W = 24.17 \tag{9}$$
$$S_B^2 = \frac{SS_B}{df_b} = 12.09$$
$$S_W^2 = \frac{SS_W}{df_W} = 0.75$$
$$F_{calculated} = \frac{S_B^2}{S_W^2} = 16.05$$
$$F_{calculated} > F_{critical}$$

In light of the above, the null hypothesis H_0 should be rejected, and the alternative hypothesis H_a should be accepted. The analysis of variance provided 99% confidence that, with the current setup, the number of sudden changes in the direction of the velocity vector of the head affects geometric inaccuracies.

Table 6

Collective data used for statistical calculations

Shape type	Cylinder, $\bar{x}_w = 43.71$			Prism with square base, $\bar{x}_t = 43.53$			Prism with triangular base, $\bar{x}_k = 44.96$		
	x_{wi}	$(x_{wi} - \bar{x}_C)^2$	$(x_{wi} - \bar{x}_w)^2$	x_{ti}	$(x_{ti} - \bar{x}_C)^2$	$(x_{ti} - \bar{x}_t)^2$	x_{ki}	$(x_{ki} - \bar{x}_C)^2$	$(x_{ki} - \bar{x}_k)^2$
1.	42.66	1.98	1.10	42.02	4.19	2.28	43.57	0.25	1.93
2.	42.71	1.84	1.00	42.09	3.91	2.08	43.59	0.23	1.87
3.	42.84	1.50	0.76	42.19	3.52	1.80	44.31	0.06	0.42
4.	42.88	1.41	0.69	42.26	3.26	1.62	44.35	0.08	0.37
5.	42.90	1.36	0.66	42.45	2.61	1.17	44.45	0.15	0.26
6.	43.02	1.09	0.48	42.80	1.60	0.53	44.48	0.17	0.23
7.	43.23	0.70	0.23	43.07	0.99	0.21	44.51	0.20	0.20
8.	43.66	0.16	0.00	43.30	0.59	0.05	44.63	0.32	0.11
9.	43.76	0.09	0.00	43.30	0.59	0.05	44.87	0.65	0.01
10.	43.79	0.08	0.01	43.50	0.32	0.00	44.93	0.75	0.00
11.	43.86	0.04	0.02	43.66	0.16	0.02	45.18	1.24	0.05
12.	43.91	0.02	0.04	43.71	0.13	0.03	45.19	1.26	0.05
13.	43.93	0.02	0.05	43.76	0.09	0.05	45.21	1.31	0.06
14.	43.94	0.02	0.05	43.78	0.08	0.06	45.27	1.45	0.10
15.	44.06	0.00	0.12	43.94	0.02	0.17	45.37	1.70	0.17
16.	44.06	0.00	0.12	44.57	0.25	1.08	45.52	2.11	0.32
17.	44.31	0.06	0.36	44.62	0.31	1.19	45.68	2.60	0.52
18.	44.37	0.09	0.44	44.68	0.38	1.32	45.75	2.84	0.63
19.	44.39	0.10	0.46	45.44	1.89	3.64	45.82	3.08	0.74
20.	45.91	3.40	4.84	45.48	2.00	3.80	46.48	5.83	2.32

5. CONCLUSIONS

Additive manufacturing using the spatial hardfacing machine constructed by the "Mechanics" science club requires adjustments in the welding speed at points where the velocity vector changes. A prolonged duration of changing the welding direction leads to shape inconsistencies, manifested as interruptions in the welding pool. This issue is caused by difficulties in maintaining a constant welding speed, along with play in the drive transmission system and a simple control system. To achieve greater geometric accuracy, it is advised to purchase an inverter welder with a wider range of adjustment and current stability, as well as to refine the control program regarding speed changes at critical points (mainly in corners).

Through the application of statistical methods, it has been demonstrated that geometric deviations are not random and depend on the number of sudden changes in the direction of the velocity vector of the welding torch. Utilizing robotic welders, as more advanced machines both kinematically and programmatically, can mitigate this inconvenience.

References

[1] Qi X., Ren Y., Wang X.: *New advances in the biodegradation of Poly(lactic)acid*. International Biodeterioration & Biodegradation 2017, 117: 215–223.

[2] Zhu Y., Tian X., Peng Li J., Wang H.: *The anisotropy of laser melting deposition additive manufacturing Ti–6.5Al–3.5Mo–1.5Zr–0.3Si titanium alloy*. Materials and Design 2015, 67: 538–542.

[3] Di L., Yiran Y.: *Cost Modeling and Evaluation of Direct Metal Laser Sintering with Integrated Dynamic Process Planning*. Sustainability 2021, 13, 1: 319, https://doi.org/10.3390/su13010319.

[4] Gratton A.: *Comparison of Mechanical, Metallurgical Properties of 17-4PH Stainless Steel between Direct Metal Laser Sintering (DMLS) and Traditional Manufacturing Methods*. National Conference of Undergraduate Research 2012 [conference materials].
[5] Cegielski P.: *Nowe obszary zastosowania napawania łukowego MIG/MAG*. Przegląd Spawalnictwa 2016, 6: 48–49.
[6] Cegielski P., Ostrysz M., Łacisz W., Panas M., Kowalski P.: *Nowe prace nad wykorzystaniem napawania łukowego MIG/MAG do drukowania 3D*. Przegląd Spawalnictwa 2018, 1: 43–47.
[7] *Sterowanie numeryczne obrabiarek*. Portal wiedzy CNC, http://cnc.pl/sterowanie-ksztaltowe.php [15.06.2021].
[8] *Modernizacja układu sterowania plotera frezującego*. Portal wiedzy CNC, http://cnc.pl/przed-cnc.php [15.06.2021].

TOMASZ GÓRAL, Ph.D., Eng.
STANISŁAW KRAWCZYK, Ph.D., Eng.
JAN PAWLIK. M.Sc., Eng.

Department of Manufacturing Systems
Faculty of Mechanical Engineering and Robotics
AGH University of Krakow
al. A. Mickiewicza 30
30-059 Krakow, Poland
{*tgoral, stkrawcz, jan.pawlik*}*@agh.edu.pl*

© 2023 Authors. This is an open access publication, which can be used, distributed and reproduced in any medium according to the Creative Commons CC-BY 4.0 License.